processes

MDPI

Article

Separation and Removal of Radionuclide Cesium from Water by Biodegradable Magnetic Prussian Blue Nanospheres

Shanshan Feng [1,2,3,*], Jie Ni [1], Xun Cao [1], Jingshuai Gao [1], Lu Yang [1], Wenhao Jia [1], Feng Chen [1], Sheng Feng [1], Yao Zhang [1,*] and Fang Ma [3,4,*]

[1] School of Environmental Science and Engineering, Changzhou University, Changzhou 213164, China
[2] Jiangsu Petrochemical Safety and Environmental Protection Engineering Research Center, Changzhou 213164, China
[3] State Key Laboratory of Urban Water Resources and Environment, Harbin 150001, China
[4] School of Environmental Engineering, Harbin Institute of Technology, Harbin 150001, China
* Correspondence: fengshanshan@cczu.edu.cn (S.F.); zyjs@cczu.edu.cn (Y.Z.); mafang@hit.edu.cn (F.M.)

Abstract: As the main component of radioactive wastewater, the cesium ion has seriously endangered the environment and human health. Prussian blue nanoparticles (PB NPs) are used as adsorbents for the purification of cesium-containing wastewater because of their ability to selectively adsorb cesium ions. In this work, novel magnetic Prussian blue nanospheres (MPBNs) were developed from polylactic acid nanospheres as a carrier, loaded with Fe_3O_4 nanoparticles (Fe_3O_4 NPs) inside and PB NPs outside for the removal of cesium ions with the help of magnetic separation. Meanwhile, the effects on the adsorption efficiency of MPBNs, such as pH, time, temperature and initial concentration of cesium ion solution, were studied. The adsorption isotherms, kinetic models and adsorption thermodynamics were investigated to research the absorption mechanism. The results showed that MPBNs were spherical with a rough surface, and their particle size, iron content and saturation magnetization were 268.2 ± 1.4 nm, 40.01% and 41.71 emu/g, which can be recovered by magnetic separation. At 293 K, MPBNs could reduce the cesium ion solution from 40 mg/L to 4.8 mg/L, and its cesium ion removal rate and adsorption capacity were 82.46% and 16.49 mg/g, respectively. The optimum pH of MPBNs for cesium ion adsorption was 5~9, the adsorption equilibrium time was 60 min, and the maximum adsorption capacity was 17.03 mg/g. In addition, MPBNs were separated rapidly by an external magnetic field, and the adsorption process was an endothermic reaction. The adsorption isotherm and kinetics of MPBNs were in accordance with the Freundlich model and quasi-second-order fitting model, respectively, and the adsorption process of MPBNs was controlled by the diffusion step in particles. Notably, these MPBNs could be effectively separated from water by a magnetic field, facilitating engineering applications in cesium-containing wastewater.

Keywords: cesium ions; degradation; magnetic separation; Prussian blue

check for updates

Citation: Feng, S.; Ni, J.; Cao, X.; Gao, J.; Yang, L.; Jia, W.; Chen, F.; Feng, S.; Zhang, Y.; Ma, F. Separation and Removal of Radionuclide Cesium from Water by Biodegradable Magnetic Prussian Blue Nanospheres. *Processes* **2022**, *10*, 2492. https://doi.org/10.3390/pr10122492

Academic Editor: Gujie Qian

Received: 26 October 2022
Accepted: 19 November 2022
Published: 23 November 2022

Publisher's Note: MDPI stays neutral with regard to jurisdictional claims in published maps and institutional affiliations.

Copyright: © 2022 by the authors. Licensee MDPI, Basel, Switzerland. This article is an open access article distributed under the terms and conditions of the Creative Commons Attribution (CC BY) license (https://creativecommons.org/licenses/by/4.0/).

1. Introduction

Nuclear energy is undergoing vigorous development towards clean energy. While alleviating the energy shortage, this also produces more and more radioactive waste water, which contains cesium, strontium and other natural radionuclides. Among these, ^{137}Cs is the primary radiological concern owing to its high fission yield, long half-life, high volatility, high activity and high solubility [1]. If ^{137}Cs cannot be effectively treated and directly discharged into the environment, it will enter the human body through diffusion and be enriched in the body. Even a small amount of cesium will harm human health. Therefore, it is very important to treat and purify cesium-containing wastewater.

The radiation characteristics of radioactive wastewater containing cesium and other pollutants will not be decomposed and destroyed by physical or chemical methods at all, and its radioactivity can only be reduced by natural decay. Thus, it is necessary to

concentrate the adsorbed pollutants and then solidify and seal them. At present, the major handling methods for cesium-containing wastewater are chemical precipitation, evaporation and concentration, ion exchange, adsorption, membrane treatment and ion flotation [2–4]. The adsorption method has become a research hotspot because of its economic price, abundant adsorbent sources, good stability, simple technology, excellent treatment effect and wide application range. Researchers are constantly committed to developing low-cost and efficient adsorption materials, especially safe and effective functional adsorption materials.

After the Fukushima Daiichi nuclear power plant leak, Prussian blue (PB) has been used for the purification and treatment of cesium, because it has a crystal cage size similar to the hydration radius of cesium ions [5]. Meanwhile, PB has the advantages of a large specific surface area, increased surface atomic number and increased surface energy. For example, Ishizaki synthesized PB NPs with the chemical formula (Fe_4 [Fe $(CN)_6]_3$) [6]. This was mainly related to the cubic configuration of the cyanide-bridged iron center of the PB internal structure, which allowed the insertion of additional cations into intergap positions, and/or ion exchange with K^+, H^+ and other bound cations [7]. Smaller hydrated cations such as Rb^+, Cs^+ and $NH_4{}^+$ were found to pierce through the structure, while similar Na^+ and Li^+ larger cations can be well blocked [8]. Torad synthesized hollow PB NPs by a self-etching reaction, which greatly increased its surface area (330 m^2/g) [9]. These nanoparticles have higher cesium ion removal performance than commercial PB. However, it can be found that using pure PB NPs to adsorb cesium creates many difficulties in the later separation process [10]. Due to its small size, small surface activity and easy aggregation, it is difficult to separate PB by centrifugation or filtration after adsorption. This will affect the light transmission of water and form pollution. Therefore, it is an urgent goal to completely remove PB NPs from water after removing cesium ions.

In order to solve the above problems, magnetic nanomaterials for adsorbent recycling were constructed, or PB NPs were fixed on different carrier surfaces through various technologies to prepare rapidly separable adsorption materials. For example, Chakrit prepared a new type of magnetic PB functional adsorbent, which had a high adsorption capacity (96 mg/g), and its saturation magnetization intensity was 20 emu/g, which can ensure that the adsorbent can be quickly separated by the external magnetic field after adsorbing cesium ions [11]. However, the adsorbent requires some improvements, such as the dispersion, aggregation, specific surface area and adsorption properties of nanoparticles. HongjunYang used calcium alginate as the carrier of magnetic Prussian blue and fixed it with graphene oxide as an adsorbent that can remove cesium ions from aqueous solutions, with the maximum adsorption amount of 43.51 mg/g [12]. Nonetheless, calcium alginate is slightly harmful to water bodies, and sewage containing calcium alginate is not allowed to be discharged without government permission. Meanwhile, the preparation process of the adsorbent is complex and is not suitable for mass production. Therefore, it is crucial to develop efficient adsorbents that are environmentally friendly and easy to separate.

Polylactic acid (PLA) has good thermal stability and ductility. It can be produced by the fermentation of starch crops and domestic garbage as raw materials. Its preparation process has no pollution, and its circulation in nature will not cause harm to the environment. In recent years, as a new type of degradable material, polylactic acid has been widely used in the textile field, biomedicine, industrial packaging, automobile industry and other fields, especially in the biomedical field. On the one hand, it is used as a carrier to load drugs for disease treatment. On the other hand, it is designed as a contrast agent for disease diagnosis. However, it is rarely used in the environmental field. Because of this, the study selected PLA as the fixed carrier of PB NPs and designed a separable Prussian blue green adsorbent to achieve the treatment of cesium-containing wastewater. Secondly, the morphology, particle size and related physical and chemical properties of the adsorbent were tested. Thirdly, the adsorption performance of the adsorbent for cesium was studied. Finally, the adsorption mechanism of the adsorbent was discussed.

2. Materials and Methods

In this work, a rapid separation and biodegradation magnetic Prussian blue nanosphere adsorbent was designed by double emulsion technique and stably assembled technique to simulate the removal of radionuclide cesium ions from water (Figure 1). We selected biodegradable polylactic acid nanospheres as a carrier, with encapsulated paramagnetic Fe_3O_4 nanoparticles inside, and grew with a diameter of 15 nm on its outer surface. Meanwhile, the morphology, particle size and related physical and chemical properties of the MPBNs were tested. Moreover, the effects of the temperature, pH, initial concentration and time on its ability to adsorb cesium ions were researched. Finally, the adsorption mechanism was discussed by combining the adsorption isotherms, adsorption kinetics and adsorption thermodynamics of magnetic Prussian blue nanospheres.

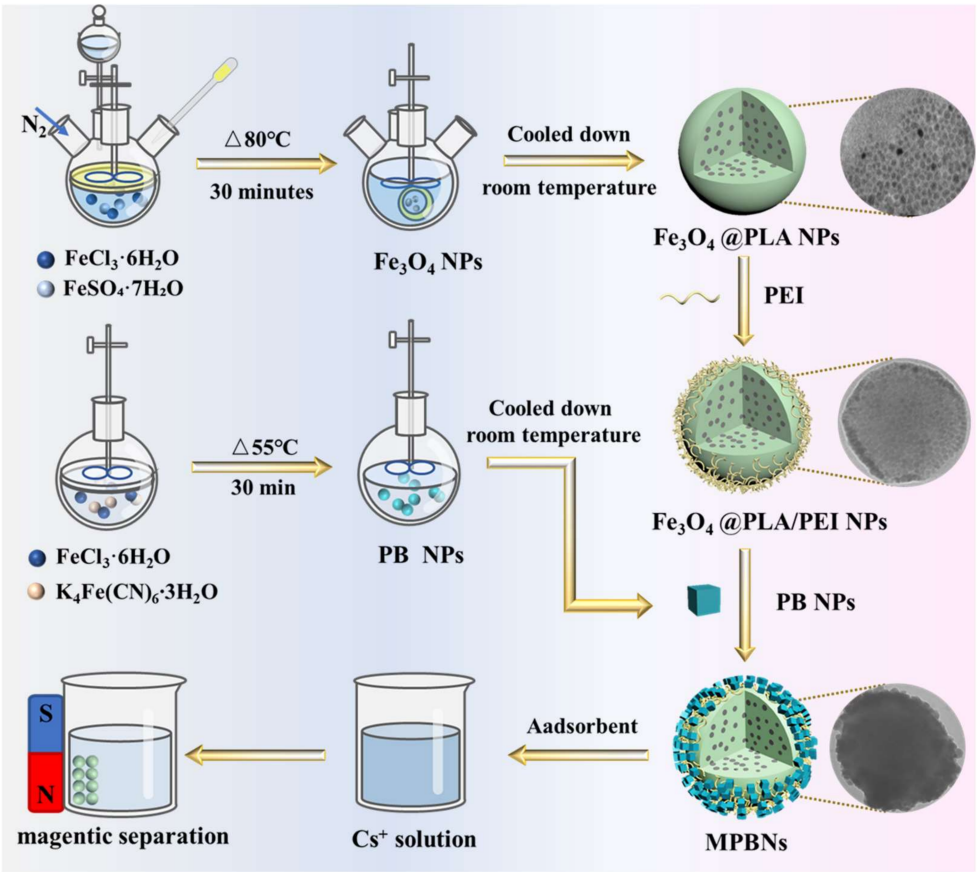

Figure 1. Schematic diagram of the preparation process of MPBSNs and their application to remove cesium ions.

2.1. Materials and Instrument

Citric acid ($C_6H_8O_7$, AR) was purchased from Kaitong Chemical Reagent Co., Ltd. (Tianjing, China). Ferric chloride ($FeCl_3$ $6H_2O$, AR), ferrous sulfate ($FeSO_4{\cdot}7H_2O$, AR) and potassium ferrocyanide (K_4Fe $(CN)_6$ $3H_2O$, AR) were purchased from Tianjin Comio Chemical Reagent Co., Ltd. (Tianjing, China). Polylactic acid ($(C_3H_4O_2)_n$, GR) was purchased from the Shandong Medical Device Research Institute. PVA ($(C_2H_4O)_n$, GR) was purchased from Tianjin Afaisha Chemical Co., Ltd. (Tianjing, China). Camphor ($C_{10}H_{16}O$, GR), polyether imide ($(C_{39}H_{30}N_2O_6)_n$, GR) and potassium bromide (KBr, AR) were purchased from Tianjin Benchmark Chemical Reagent Co., Ltd. (Tianjing, China). Methylene chloride (CH_2Cl_2, AR), pure isopropyl alcohol (C_3H_8O, AR), sodium chloride (NaCl, AR), pure potassium dihydrogen phosphate (KH_2PO_4, AR), ammonium chloride (NH_4Cl, AR), potassium chloride (KCl, AR), aqueous ammonia (NH_3 H_2O, AR), acetone (CH_3COCH_3, AR)

and pure oleic acid ($C_{18}H_{34}O_2$, AR) were purchased from Sinopharm Chemical Reagents Co., Ltd. (Shanghai, China). All water used in the experiment was deionized water (18.2 MΩ·cm) from the Milli-Q system.

At first, an electronic balance was used to weigh the drugs (BS124S, Sardolis, Germany). Secondly, the drug was evenly dispersed in the solution using a mechanical agitator (RW20, IKA, Staufen, Germany), a water bath ultrasonic cleaner (DL-360D, Shanghai Zhixin Instrument Co., Ltd., Shanghai, China), a vortex oscillator (VERTEX-5, Jiangsu Haimen Kirinberg Instrument Manufacturing Co., Ltd., Haimen, China) and a shaker. Then, a centrifuge (2-16PK, SIGMA) was used for material collection. Finally, a vacuum freeze dryer (TFD5505, SIM Company, Los Angeles, CA, USA) and vacuum drying oven (DZF-6020, Shanghai Experimental Instrument General Factory, Shanghai, China) were used to dry the drugs.

2.2. Fabrication of Magnetic Prussian Blue Nanospheres

2.2.1. Preparation of Fe_3O_4 Nanoparticles (Fe_3O_4 NPs)

Magnetic Fe_3O_4 NPs were synthesized by the solvothermal technique. First of all, 13.2 g of $FeCl_3$ $6H_2O$ and 8.0 g of $FeSO_4 \cdot 7H_2O$ were added to a 250 mL four flask, and we injected nitrogen into the flask to remove the oxygen. Then, we added 100 mL of deionized water into the flask, stirred it with high-speed mechanical stirrer to make it dissolve quickly, dropped slowly 40 mL of ammonia into the flask using a constant pressure drop funnel, and heated the reaction system to 80 °C [13,14]. Next, we added 5 mL of oleic acid drop by drop to the reaction system, kept heating it for 30 min after dropping, and then stopped heating and cooled it to room temperature. After this, the nanoparticles were separated with magnets and washed three times with deionized water and ethanol, respectively. Finally, we dispersed the nanoparticles in n-hexane, known as magnetic Fe_3O_4 NPs, and placed them in a refrigerator at 4 °C for sealing.

2.2.2. Preparation of Prussian Blue Nanoparticles (PB NPs)

PB NPs were synthesized by a modified hydrothermal method. Briefly, 1 mmol of $FeCl_3$ and K_4Fe $(CN)_6$ were added to 20 mL and 5 mmol of citric acid aqueous solution, respectively. We ensured that the molar ratio of $FeCl_3$ and K_4Fe $(CN)_6$ to citric acid in the system was 5:1 and stirred the mixture with a magnetic stirrer to allow it to fully dissolve [15]. The aqueous solution of ferric chloride containing citric acid was heated to 55 °C. Then, 20 mL of aqueous solution containing citric acid and potassium ferrocyanide, with molar masses of 0.05 mM and 1 mM, respectively, was rapidly added to the above solution. After dropping, the solution was kept heated for 30 min, and then cooled to room temperature. An equal volume of acetone was added to the reaction system, mixing and standing at room temperature for 30 min. Later, we centrifuged it at a low temperature and high speed (15,000 rpm, 30 min), removed the supernatant carefully after collecting the precipitate, washed it with deionized water, added an equal volume of acetone, and centrifuged it again. This process was repeated three times, and 15 nm PB NPs could be obtained, which were stored in a refrigerator at 4 °C until use [16].

2.2.3. Preparation of Magnetic Nanospheres (Fe_3O_4@PLA NPs)

The resulting Fe_3O_4@PLA NPs were prepared by the double emulsion method. In brief, we dissolved 100 mg of PLA in 4mL of methylene chloride at room temperature. Then, a suspension of n-hexane containing Fe_3O_4 NPs (V: 0.5 mL, C: 20 mg/mL) was added as the organic phase solution [17]. Next, the organic phase solution was added drop by drop into the PVA solution precooled in a 4 °C refrigerator (V: 20 mL, wt.%: 2%), and it was ultrasonically treated in the ice bath for two minutes with a sonic cell crushing apparatus to form oil-in-water (O/W) nanospheres [18]. Following this, the solution was placed in a ventilated kitchen and stirred for 3 h to ensure the rapid volatilization of organic solvents in the system. After waiting for organic solvent volatilization, the emulsion was centrifuged (15,000× *g*, 5 min, 5 °C); we discarded the supernatant solution and retained the precipitate,

using deionized water under vortex shaking and water bath ultrasonic separation; this process was repeated three times. Finally, we collected the precipitate using a deionized water dispersion, kept some for lower operation, and placed the rest in the lyophilizer (−54 °C, 36 h) for freeze drying. Fe_3O_4@PLA NPs could be obtained, which were sealed and stored at −20 °C for later use.

2.2.4. Preparation of Magnetic Prussian Blue Nanospheres (MPBNs)

The MPBNs in this work were prepared by classical assembly techniques. At the beginning, 1 mL of magnetic nanosphere suspension was added into PEI solution (V: 100 mL, C: 2 mg/mL, prepared with 0.5 mol/L NaCl solvent), placed in a shaker for adsorption for 20 min, and centrifuged (5000× *g*, 5 min, 15 °C). The supernatant was discarded to collect the precipitate, and deionized water was added for eddy dispersion. After two centrifugal washing steps, unabsorbed PEI molecules in the solution were washed. Then, 25 mL and 2 mg/mL PB NP suspension were added and placed in a shaker for mixed adsorption for 20 min. In the end, the samples were separated and washed 3 times with the help of magnets. The concentrated solution was freeze-dried in lyophilized water (−54 °C, 36 h) to obtain MPBNs, and the samples were sealed and stored at −20 °C for later use.

2.3. Instrumentation and Characterization of Adsorbent

Firstly, a dynamic light scattering laser particle size analyzer and a zeta potentiometer (Bi-ZetaPlus/90Plus, Brookhaven, NY, USA) were used to monitor the changes in particle size and surface potential during the preparation of the samples. Then, the morphology and elemental content of the prepared samples were tested using transmission electron microscopy and EDS spectroscopy (H7650, Hitachi, Japan). Secondly, hysteresis loops of the prepared magnetic samples were tested using a magnetometer (7307, Lakeshore, LA, USA). At the same time, an X-ray energy spectrum analyzer (XRD, Rigaku Co., Tokyo, Japan) and Fourier infrared spectroscopy analyzer (FTIR, Varian FTS 3100, Galloway, OH, USA) were used to successively characterize the crystal diffraction and functional groups of the prepared samples. In addition, the change in cesium ion concentration before and after the experiment was measured by means of inductively coupled plasma emission spectroscopy (ICP-OES, Agilent 7500CE, Palo Alto, CA, USA).

2.4. Batch Adsorption Experiments

2.4.1. Adsorption Experiment

In the study of optimal adsorption conditions, the intermittent adsorption method was adopted. Firstly, 1.2668 g cesium chloride was dried overnight in a muffle furnace at a high temperature (105 °C) and dissolved in a small amount of deionized water. Then, 1 mg/mL cesium ion stock solution was prepared for the configuration of different cesium ion concentrations in the adsorption experiment. Then, the effects of the initial concentration, temperature, time, pH value and adsorbent dosage on cesium ion adsorption were studied. The main steps were as follows: a certain amount of MPBN and Cs^+ solution was placed into a beaker, and the pH was adjusted with hydrochloric acid (0.1 mol/L) and sodium hydroxide solution (0.1 mol/L), and it was then placed on a constant-temperature shaking table at 200 rpm for adsorption. We separated the adsorbent from the cesium ion aqueous solution and determined the cesium ion concentration after separation by ICP-OES. Three parallel samples were required for each sample to consider the influence of different conditions on the adsorption effect.

2.4.2. Recovery of Adsorbents

The adsorption experiments applied different doses of magnetic adsorbent after the completion of magnetic separation recovery. We placed the magnetic adsorbent in a vacuum oven overnight to dry (55 °C, 12 h), and then used an electronic balance to weigh the quality of the dry adsorbent; we calculated, according to the adsorbent additive quantity changes before and after the reaction, the recovery rate of the adsorbent.

2.4.3. Sedimentation Experiments on MPBNs

The sedimentation experiment on the prepared MPBNs was carried out as follows: two measuring cylinders of 50 mL were taken, magnetic samples with an equal volume concentration of 30 mg/L were added, and the samples were stirred evenly with a glass rod and left to ensure the dispersion of particles in the liquid. Then, a magnet was placed under one cylinder while the other one was not placed, and the gravity and magnetic force were used to settle it, respectively. Then, the height and corresponding time of the magnetic sample were recorded rapidly.

2.4.4. Calculation of Adsorption Data

The adsorption capacity of MPBNs on cesium ions was described via the adsorption rate and adsorption quantity [19]. The adsorption rate R (%) of cesium and the adsorption capacity Q (mg/g) of adsorbent were calculated according to the concentration of cesium before and after adsorption. The cesium adsorption rate of MPBNs was calculated according to Equation (1), and the adsorption capacity of MPBNs was calculated according to Equation (2).

$$R\% = \frac{C_0 - C_i}{C_0} \times 100\% \quad (1)$$

$$Q_e = \frac{C_0 - C_e}{m} \times V \quad (2)$$

where R (%) is the adsorption rate of MPBNs to cesium element; C_0 (mg/L) is the mass concentration of cesium before adsorption; C_i (mg/L) is the mass concentration of cesium at adsorption time i; Q_e (mg/g) is the adsorption capacity of MPBNs; C_e (mg/L) is the mass concentration of cesium after adsorption equilibrium; m (mg) is the quality of MPBNs; V (L) is the volume of cesium ions.

3. Results and Discussion

3.1. The Formation Mechanism of MPBNs

In this paper, Prussian blue was loaded on the surface of the biodegradable carrier, namely polylactic acid nanospheres, and ferric tetroxide was wrapped inside the nanospheres to prepare magnetic Prussian blue nanospheres (MPBNs), using the double-emulsion method and electrostatic assembly process, as shown in Figure 1. Firstly, Fe_3O_4 NPs with a particle size of approximately 5 nm were prepared by the solvothermal method. As shown in Figure 2a, TEM images showed that the shape of Fe_3O_4 NPs was nearly circular, uniformly dispersed without aggregation, and the particle size was approximately 5 nm. Then, magnetic lactate nanospheres (Fe_3O_4@PLA NPs) were prepared by means of the oil-in-water emulsified solvent volatilization process. Ferric tetroxide was wrapped in the interior of the polylactic acid nanospheres. In other words, polylactic acid and ferric tetroxide were taken as organic phases and polyvinyl alcohol was taken as the aqueous phase. The oil-in-water emulsion was formed by ultrasonic cell fragmentation technology, and the magnetic degradable polylactic acid nanospheres with a negative surface charge were finally obtained. In addition, the modified hydrothermal method was used to prepare PB NPs with a diameter of 15 nm, and citric acid was added as a protective agent to regulate the content of ferric chloride and potassium ferrocyanide, so as to regulate the size of PB NPs and negatively charge the surface, and to improve the dispersibility on the surfaces of the polylactic acid nanospheres. Finally, electrostatic adsorption technology was used to adsorb negatively charged PB NPs on the surfaces of the magnetic polylactic acid nanospheres with the help of the electrolyte PEI with a positive charge, and the PB NPs were evenly distributed and firmly fixed on the surfaces of the magnetic nanospheres, which had good cesium ion selectivity. After this, freeze-drying technology was used to remove the aqueous phase in the nanospheres, so that the ferric tetroxide was better wrapped in the inside of the spheres, which had good magnetic separation characteristics and obtained a lyophilized powder. In this way, a new multifunctional cesium adsorbent, MPBNs, was obtained.

3.2. Characterization of Physicochemical Properties of MPBNs

3.2.1. Morphology Analyses of MPBNs

To enhance the adsorption capacity of cesium ions and increase the loading content of PB in the polylactic acid nanospheres, according to the size effect and surface area effect of nanoparticles, reducing the particle size of PB NPs will increase the specific surface area of PB NPs, which can increase the fixed content of PB NPs in nanospheres. In this study, PB NPs with a diameter of 15 nm were prepared by regulating the content of citric acid and Fe^{2+}/Fe^{3+} at 55 °C [20]. As shown in Figure 2b, TEM images of PB NPs revealed that the shape of PB NPs was nearly circular, which was mainly due to the incomplete crystal on the particle surface caused by the increase in citric acid. Moreover, PB NPs were uniformly dispersed without aggregation, and the particle size was between 10 nm and 20 nm. Meanwhile, the average particle size of PB NPs measured by DLS was 16.36 ± 2.45 nm, and no larger particle size was found (Figure 3a).

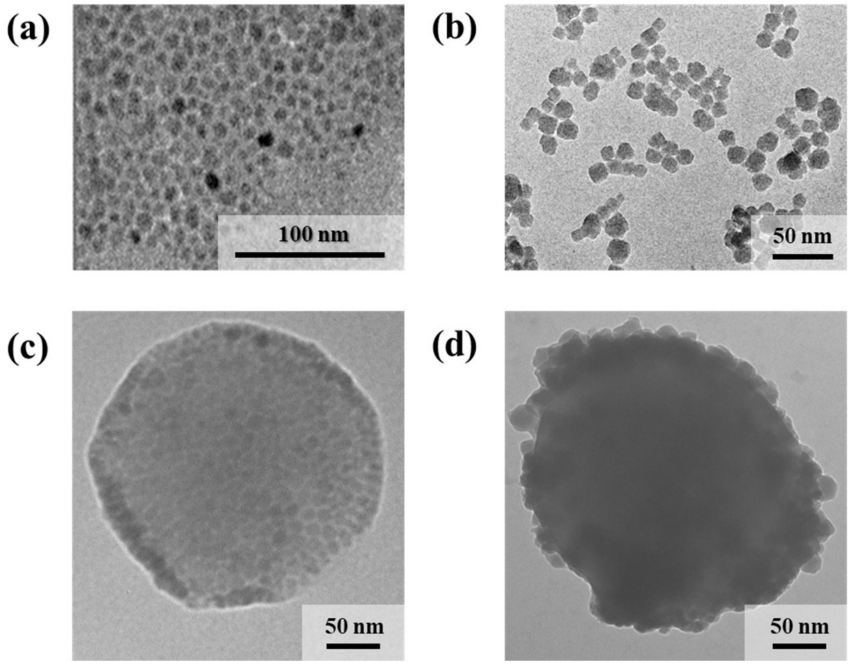

Figure 2. The TEM images of (**a**) Fe_3O_4 NPs; (**b**) PB NPs; (**c**) Fe_3O_4@PLA NPs, and (**d**) MPBNs.

Subsequently, Figure 2c shows that Fe_3O_4@PLA NPs without PB NPs were spherical in shape, with a particle size range of approximately 300 nm, and many fine particles were closely arranged inside, which were Fe_3O_4 NPs. Moreover, Figure 3b shows that the Fe_3O_4@PLA NPs were normally distributed and evenly dispersed, with an average size of around 253.4 ± 2.3 nm. Then, after loading PB NPs (Figure 2d), MPBNs were still completely spherical with a rough surface, and many PB NPs could be clearly seen distributed on the surfaces of the nanospheres. Meanwhile, the average particle size of magnetic nanospheres modified by PB NPs was 268.2 ± 1.4 nm, and the particle size distribution is shown in Figure 3c. However, the particle size of Fe_3O_4@PLA NPs increased by approximately 15 nm after the electrostatic adsorption of PB, which was mainly due to the increase in size caused by the surface modification of PB NPs. Moreover, the structure of the nanospheres did not change after modification, indicating that magnetic nanospheres had good stability, which was more conducive to removing cesium ions from aqueous solutions [21]. The results of TEM and DLS showed that PB NPs were deposited on the surfaces of Fe_3O_4@PLA NPs by electrostatic action, and MPBNs were successfully prepared.

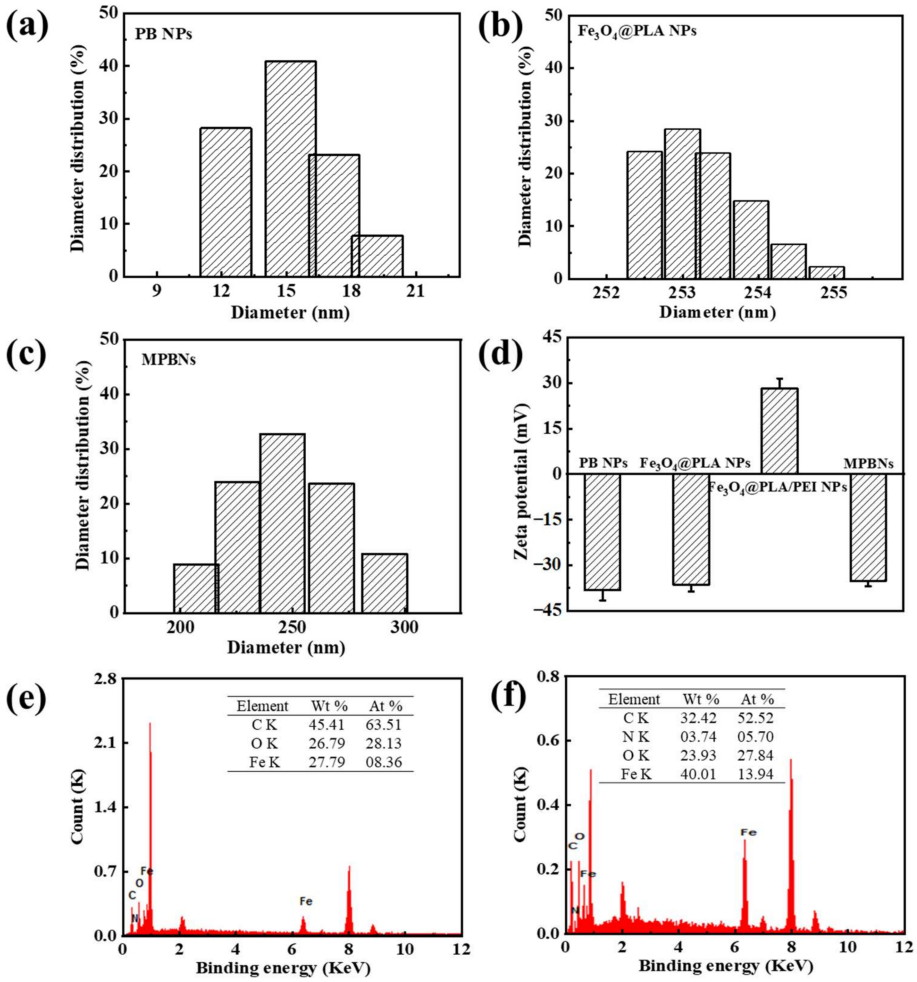

Figure 3. The size distribution of (**a**) PB NPs; (**b**) Fe_3O_4@PLA NPs; and (**c**) MPBNs. The zeta potential of the fabrication process of (**d**) MPBNs; EDS spectra of (**e**) Fe_3O_4@PLA NPs (**f**) and MPBNs.

3.2.2. Zeta Analyses of MPBNs

MPBNs were prepared by using degradable polylactic acid nanospheres (PLA NPs) as the carrier of PB NPs, which could be suspended and separated. In addition, Fe_3O_4 NPs were embedded in PLA NPs to speed up the separation of the adsorbent and reduce the use of the treatment space. As shown in Figure 3d, the surface potential changes of the samples in different periods also verified that PEI and PB NPs were assembled on the surfaces of MPBNs in turn. Firstly, the surface potential of PB NPs measured by the zeta potentiometer was approximately -38.28 ± 3.34 mV (Figure 3d), with a strong negative charge, which guaranteed that the particles produced a certain electrostatic repulsion and stably existed in the aqueous solution. Then, the zeta potential analyzer detected that the Fe_3O_4@PLA NPs' zeta potential was -36.47 ± 2.29 mV, which was caused by the presence of carboxyl groups on the surface. At this point, it was necessary to adsorb a layer of positively charged PEI on the surface of Fe_3O_4@ PLA NPs to assemble negatively charged PB NPs. Then, the zeta potential of Fe_3O_4@PLA NPs after PEI adsorption was 28.39 ± 3.19 mV. Finally, the PB NPs were mixed with Fe_3O_4@PLA/PEI NPs, and the zeta potential was -35.23 ± 1.59 mV, indicating that PB NPs had been successfully bound to the surface of Fe_3O_4@PLA NPs.

3.2.3. Element Content Analyses of MPBNs

The elemental changes of Fe_3O_4@PLA NPs before and after the adsorption of PB NPs were analyzed. It can be seen from Figure 3e that the spectral peaks of Fe_3O_4@PLA NPs were mainly C, O, and Fe (except Au), and the percentages of the three elements in the

total element mass were 45.41%, 26.79%, and 27.79%, respectively. The carbon element was derived from the PLA NP carrier, the iron element was from the Fe_3O_4, and the oxygen element was from the PLA NPs and the Fe_3O_4, respectively. Moreover, according to the EDS spectrum of MPBNs shown in Figure 3f, it can also be observed that there were three element spectral peaks of C, O, and Fe, and the percentages of the three elements in the total element mass were 32.42%, 27.57%, and 40.01%, respectively. The comparison between the two showed that the content of iron in the sample after adsorbing PB NPs increased, and the iron mass accounted for approximately 12.22% of the total element mass (except Au), which proved that the PB NPs were successfully adsorbed on the surfaces of the nanospheres.

3.2.4. Functional Group Structure Analysis of MPBNs

In this experiment, we revealed the functional group structure of MPBNs, which has important guiding significance in exploring the adsorption mechanism. As can be seen from the FT-IR spectrum of MNPBS in Figure 4a, strong absorption peaks were found at 1610 cm^{-1} and 2090 cm^{-1}. The characteristic absorption peak at 1610 cm^{-1} was caused by the stretching vibration of -COO- in the citric acid modified by the PB surface [22]. Moreover, the absorption peak at 2090 cm^{-1} was caused by the stretching vibration of Fe^{2+}-CN-Fe^{3+} in PB, but the intensity of the characteristic peak decreased relative to the pure PB control, which was mainly caused by the decrease in the content of PB in MPBNs. In addition, the characteristic peak at 570 cm^{-1} was caused by the stretching vibration of Fe-O in Fe_3O_4 NPs. The characteristic absorption peaks at 866 cm^{-1}, 2990 cm^{-1}, 1090 cm^{-1}, and 1760 cm^{-1} were from the =C-H, -C-C-, -C-O, -C=O groups in Fe_3O_4@PLA NPs [23]. Therefore, these vibration peaks were consistent with the characteristic peaks of PB NPs, Fe_3O_4 NPs, and Fe_3O_4@PLA NPs, and these characteristic peaks directly confirmed that PB NPs were successfully modified on the surfaces of MPBNs, indicating that the MPBNs possessed the structural characteristics of Fe_3O_4@PLA NPs, PB NPs, and Fe_3O_4 NPs.

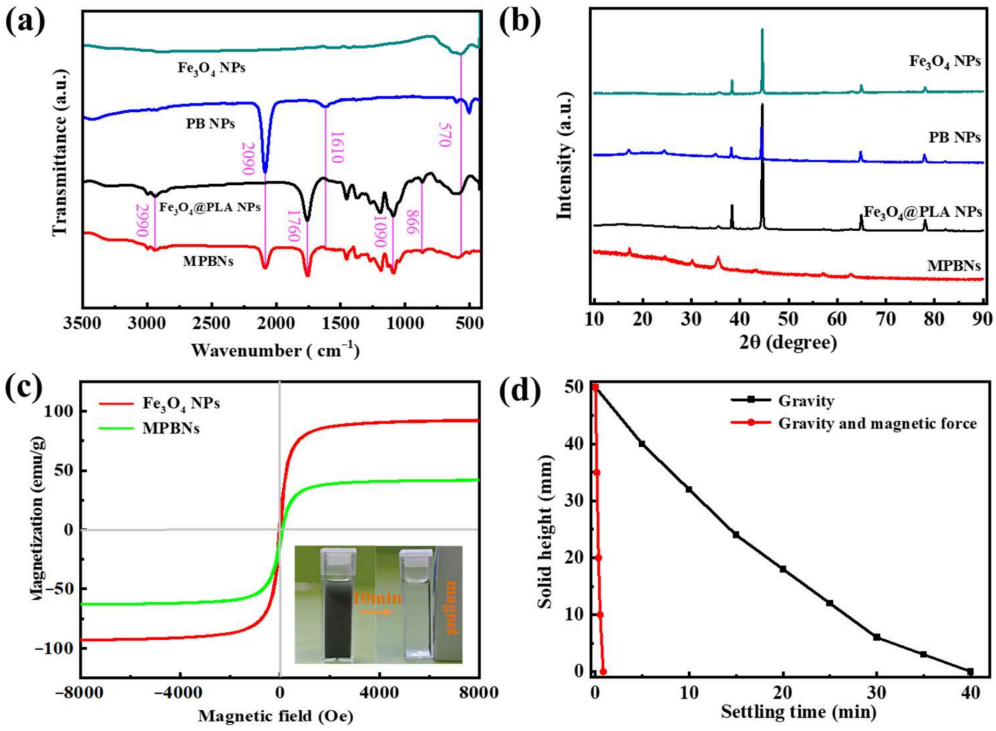

Figure 4. (**a**) FT-IR spectrum and (**b**) XRD patterns of PB NPs, Fe_3O_4 NPs, MPBNs, and Fe_3O_4@PLA NPs; hysteresis curves of Fe_3O_4 NPs and MPBNs; (**c**) photographs of MPBN suspension before and after magnet adsorption; (**d**) the test of settlement property of MPBNs in water.

3.2.5. Crystal Structure Analyses of MPBNs

The XRD was used to analyze the crystalline phase of MPBNs, as shown in Figure 4b, with the scanning range of 5~80°. The results showed that the MPBNs had diffraction peaks at 2θ = 17.59°, 24.92°, 30.14°, 35.55°, 43.17°, 57.15°, and 62.7°. Then, there were five obvious characteristic diffraction peaks in the Fe_3O_4 crystal structure at 2θ = 30.14°, 35.55°, 43.17°, 57.15°, and 62.7°. They corresponded to the three-dimensional crystal planes of Fe_3O_4 at (220), (311), (400), (511), and (440), which indicated that the product contained an anti-spinel cubic structure. Then, there were four obvious characteristic diffraction peaks at 17.59°, 24.92°, 35.57°, and 39.89°, which corresponded to the stereoscopic crystal planes of PB, respectively [24,25]. In addition, amorphous diffraction peaks were found in the range of 15~25°, which belonged to PLA NPs, which was essentially in line with the previous reports [26]. However, the intensity of these characteristic peaks decreased slightly, because, in the same mass of the original sample, MPNBs were composed of PLA NPs, Fe_3O_4 NPs, and PB NPs. All of them occupied a part of the mass and forced the intensity of the peak to decrease. However, the appearance of these characteristic peaks directly indicated that PB NPs were successfully assembled on the surfaces of MPNBs.

3.2.6. Magnetic Separation Performance of MPBNs

To realize the rapid separation of the adsorbent after adsorption, Fe_3O_4 NPs were added in the production process, so a vibration sample magnetometer was used to characterize the magnetization intensity of nanoparticles under different magnetic field intensities. It can be seen from the analysis of Figure 4c that the prepared Fe_3O_4 NPs and MPBNs had high saturation magnetization at room temperature [27]. The saturation magnetization of Fe_3O_4 NPs was 92.49 emu/g, and that of MPBNS was 41.71 emu/g. Moreover, the saturation magnetization of Fe_3O_4 NPs wrapped in MPBNs decreased to 54.9% of Fe_3O_4 NPs. This may be because Fe_3O_4 NPs were wrapped in PLA NPs, and the total content of Fe_3O_4 NPs in the sample of the same mass decreased accordingly, which led to a decrease in magnetism, but the MPBNs still had good superparamagnetism.

In addition, the MPBNs were dispersed in an aqueous solution and separated by a magnet to observe the change in MPBNs under the action of a magnetic field. From Figure 4c, it can be seen that the MPBNs were uniformly dispersed in the aqueous solution, and the suspension color was close to blue–black, which was mainly caused by the Fe_3O_4 NPs embedded in the suspension of MPBNs and the PB NPs loaded on the surface. At the same time, the MPBN particles were well dispersed in the solution, without aggregation and precipitation, which helped the MPBNs to evenly distribute in the water body and effectively adsorb cesium ions. After 10 min of magnet adsorption, MPBNs were obviously concentrated on one side of the magnet, while the solution on the side away from the magnet became clear and transparent. The results show that the Fe_3O_4 NPs in the structure endowed MPBNs with superparamagnetism, which could be removed by magnetic separation after adsorbing cesium ions, thus achieving the purpose of treating radioactive wastewater containing cesium and avoiding the generation of secondary pollution [28].

3.2.7. Settlement Performance Analysis of MPBNs

In order to investigate the deposition performance of MPBNs in water, gravity and magnetic separation were used to reveal the sedimentation characteristics of MPBNs. The contrast curve of the MPBNs' deposition time is shown in Figure 4d. When the MPBN was completely deposited at the bottom of the cylinder, it took 40 min to deposit under the action of gravity, but only 50 s for complete settlement under the combined action of gravity and magnetism. In other words, the combined gravity and magnetic force of MPBNs required a 48th of the time of the gravitational field. Because of this, the applied magnetic field could significantly increase the separation speed of MPBNs in aqueous solution. In this case, the effect of gravity on the deposition was much smaller than that of the magnetic field. Therefore, after the application of the magnetic field, the magnetic force replaced gravity as the main driving force of settlement, which greatly shortened the

time required for settlement, and this method has good separation application prospects regarding the actual process.

3.3. Adsorption-Influencing Factors of MPBNs

3.3.1. Effect of Initial Concentration on Adsorption of Cesium Ions

In wastewater treatment, the concentration of pollutants in water will affect the adsorption capacity of adsorbents, so the influence of different initial concentrations on the adsorption of cesium ions was studied. As can be seen from Figure 5a, under the same conditions, when the initial concentration was 5 mg/L, the cesium ion removal rate of MPBNs was 95.07 ± 2.78%, the adsorption capacity of MPBNs was 1.19 mg/g, and the residual concentration was approximately 0.25 mg/L. When the initial concentration was 40 mg/L, the removal rate of MPBNs increased to 82.46 ± 1.27%, the adsorption capacity of MPBNs increased to 16.49 mg/g, and the residual concentration was approximately 4.8 mg/L. The influence of the initial concentration of cesium ions on adsorption was mainly shown in the following ways. Firstly, when the initial concentration of cesium ions was less than 10 mg/L, the removal rate of cesium ions by MPBNs was more than 90%. This was because there was enough PB on the surface of MPBNs to adsorb a small amount of cesium ions in the solution. Moreover, the excess PB had not reached its saturation value, and it could continue to combine with cesium ions. Therefore, MPBN has a high removal rate of cesium ions at a low concentration [29]. Secondly, with the increase in the initial concentration of cesium ions, its removal rate started to decrease. This was attributed to the increase in the initial concentration of cesium ions, as the amount of cesium in the solution began to increase. The adsorption of these cesium ions requires more PB on the surface of MPBNs, and more and more MPBNs reach their saturation value of adsorption capacity during the adsorption process. As a result, the higher the initial concentration of cesium ions, the lower the removal rate of cesium ions by the adsorbent.

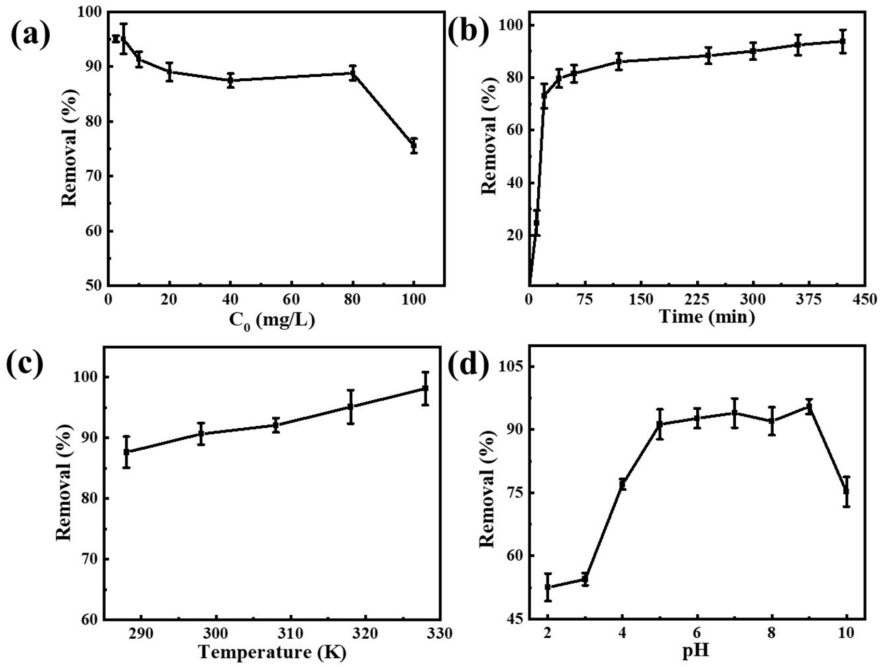

Figure 5. (**a**) Effect of initial concentration on the removal rate of cesium ions by MPBNs (pH = 5.5; m = 30 mg; V = 40 mL; T = 293 K; t = 12 h); (**b**) effect of adsorption time on the removal of cesium ions by MPBNs (C_0 = 40 mg/L; pH = 5.5; m = 30 mg; V = 20 mL; T = 293 K); (**c**) effect of temperature on the removal of cesium ions by MPBNs (C_0 = 40 mg/L; pH = 5.5; m = 30 mg; V = 20 mL; t = 12 h); (**d**) effect of pH on the removal rate of cesium ions by MPBNs (C_0 = 40 mg/L; T = 293 K; m = 30 mg; V = 40 mL; t = 12 h).

3.3.2. Effect of Time on Adsorption of Cesium Ions

In the adsorption experiments, different treatment times had an important effect on the removal efficiency of cesium ions. It can be seen from Figure 5b that the adsorption of cesium ions by MPBNs could be divided into two stages. The first stage was 20 min after the oscillation. At this stage, the removal rate of cesium ions increased rapidly, reaching 73.04 ± 4.62%. In other words, MPBNs had a fast adsorption rate, mainly because there were many vacancies in PB on the surface of the adsorbent at the initial stage of adsorption, and cesium ions were easily adsorbed. The second stage was a gradual adsorption that gradually tended towards equilibrium. Meanwhile, the speed of MPBNs adsorbing cesium ions slowed down. When the time reached 60 min, the adsorption process remained stable and gradually reached equilibrium. At this time, the removal rate was 81.52 ± 3.25%. This can be attributed to the fact that with the extension of time, many cesium ions had been adsorbed on the surfaces of MPBNs, and the vacancies in PB that could be supplied were reduced [30], which hindered the exchange of cesium, and the MPBNs reached saturation adsorption too.

3.3.3. Effect of Temperature on Adsorption of Cesium Ions

Temperature is an important factor in the adsorption process, and the removal of cesium ions will be affected by different adsorption temperatures. The results in Figure 5c show that under the same cesium ion concentration, when the temperature was 288 K, 298 K, 308 K, 318 K, and 328 K, respectively, the removal efficiency of cesium ions was 87.63 ± 2.57%, 90.66 ± 1.78%, 92.08 ± 1.18%, 95.10 ± 2.77%, and 98.13 ± 2.73%. The results showed that the removal rate of cesium ions increased gradually with the increase in temperature, indicating that the adsorption process was an endothermic reaction [31]. Furthermore, the removal rate of cesium ions was higher than 90% when the temperature was greater than 298 K. As a result, when considering energy savings and cost reduction, 298 K is a more appropriate adsorption treatment temperature in practical application. Lastly, the results showed that the binding of MPBNs to cesium ions was very stable, which was not affected by the increase in temperature.

3.3.4. Effect of pH on Adsorption of Cesium Ions

It is necessary to study the influence of the pH value on cesium ion adsorption. On the one hand, the change in pH may affect the structure of MPBNs. On the other hand, it may also affect the existing form of cesium ions, and further change the interface interaction between MPBNs and cesium ions to affect the removal efficiency of cesium ions. To investigate the influence of pH, 40 mL of cesium ion solution with a concentration of 40 mg/L was treated with 30.0 mg MPBNs under different pH conditions (2.0~10.0). The experimental results showed that the pH value had a certain impact on the adsorption of cesium ions by MPBNs at the same concentration, as shown in Figure 5d. When the pH increased from 2.0 to 3.0, the removal efficiency of MPBNs for cesium ions was less than 60%, which was mainly because there were more H^+ ions in the solution at a low pH [32]. Moreover, it was found that the functional group -COOH in MPBNs was protonated when analyzing the physical properties, and the surface mainly existed in the form of Fe (II,III)-COOH+ 2 (Equation (3)), which generated electrostatic repulsion with the cations in the solution, thus preventing the contact of positively charged cesium ions. At this time, the adsorption capacity of cesium ions was weak and the removal rate of cesium ions was relatively low.

$$Fe\,(II,III) - COOH + H^+ \rightarrow Fe\,(II,III) - COOH_2^+ \quad (3)$$

When the pH increased from 3.0 to 5.0, the removal rate of cesium ions by MPBNs increased sharply; this was mainly due to the decrease in H^+ in the solution with the increase in pH. At this time, the protonation of MPBNs was weakened, the deprotonation

of MPBNs occurred, and cesium ions were exchanged with hydrogen ions to fill the vacancy structure of PB and improve the removal efficiency of cesium ions.

When the pH was 6.0, 7.0, 8.0, and 9.0, the cesium ion removal rates of MPBNs were 92.71 ± 2.35%, 93.96 ± 3.49%, 92.00 ± 3.32%, and 95.01 ± 1.77%, respectively. With the increase in pH, the cesium ion removal rate of MPBNs almost remained stable and had no significant change. This was due to the dissociation of Fe (II,III)-COOH (Equation (4)) and the presence of Fe (II,III)-COO^- (Equation (5)) on the surfaces of MPBNs, which could combine with more positively charged cesium ions. Thus, the exchange reaction of hydrogen ions was promoted and the removal rate of cesium ions was increased, indicating that MPBNs had a higher adsorption capacity for cesium ions at this time.

$$Fe\ (II,III) - COOH \rightarrow Fe\ (II,III) - COO^- + H^+ \quad (4)$$

$$Fe\ (II,III) - COO^- + Cs^+ \leftrightharpoons Fe\ (II,III) - O - Cs \quad (5)$$

When the pH was higher than 9, the removal efficiency of cesium ions by MPBNs rapidly decreased to 75.23 ± 3.49%. In other words, with the increase in pH, the removal efficiency of cesium ions by MPBNs began to decrease. This was mainly because there were many OH^- in the solution, and Fe^{2+} and Fe^{3+} in the PB structure on the surface of the adsorbents reacted with OH^-, which changed the structure of the adsorbents. Moreover, cesium ions could easily hydrolyze to form hydroxides at this time, leading to a decrease in their adsorption efficiency. Therefore, in the actual water treatment application, considering factors such as simplicity, convenience, and economy, the appropriate pH value for removal would be 5.0~9.0.

3.3.5. Effect of Dosage on Adsorption of Cesium Ions

In the process of adsorption, the amount of adsorbent will also have a certain effect on the removal of cesium ions. Figure 6a shows the change curve of the Cs^+ removal rate under different dosages. The results suggested that the larger the dose of MPBNs, the better the removal effect of cesium ions. When the dosage of MPBNs was 10 mg, the cesium ion removal rate was only 24.67 ± 3.86%. When the dosage of MPBNs was 30 mg, the removal rate of cesium ions increased rapidly, reaching 82.46 ± 1.27%. Finally, when the dosing quantity increased to 50 mg, the removal rate of cesium reached 98.88 ± 2.46%. This is because, with the continuous increase in MPBNs, the number of reactive active sites increased, and the effective area in contact with cesium ions in the solution increased, so that more cesium ions in the solution were adsorbed by the MPBNs, and the removal rate gradually increased [33]. However, in practical applications, it is not the case that the greater the adsorbent amount, the better; the dosage of MPBNs should be selected according to the actual concentration of cesium ions in the wastewater.

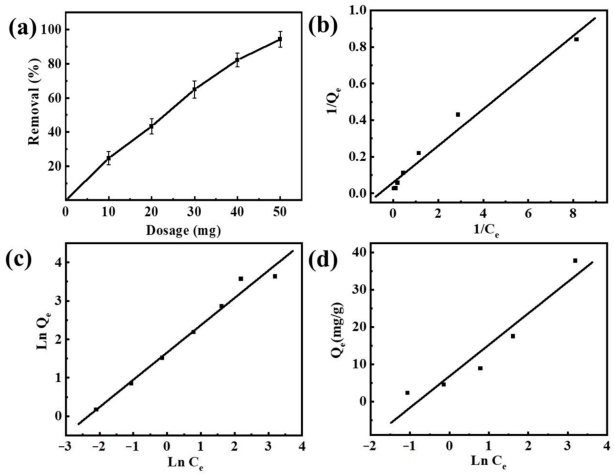

Figure 6. (**a**) Effect of MPBN dosage on the removal rate of cesium ions (C_0 = 40 mg/L; T = 293 K;

pH = 5.5; V = 40 mL; t = 12 h); (**b**) the Langmuir adsorption isotherm for cesium ion removal by MPBNs; (**c**) the Freundlich adsorption isotherm for cesium ion removal by MPBNs; (**d**) the Temkin adsorption isotherm for cesium ion removal by MPBNs.

3.4. Adsorption Isotherms of MPBNs

To describe the adsorption mechanism of adsorbents, three commonly used adsorption isotherm equations, namely the Langmuir, Freundlich, and Temkin models, were selected to fit the adsorption data in the experimental process. The Langmuir isotherm assumes that the adsorbate on the surface of the adsorbent belongs to monolayer adsorption, and the adsorption site of each adsorbent is evenly distributed [34]. When the adsorbent adsorbs the adsorbate, with the continuous increase in adsorption time, the adsorbent reaches saturation, and its adsorption capacity will remain unchanged. Its calculation equation is as follows; see Equation (6). The linear expression of Langmuir's adsorption isotherm is shown in Equation (7).

$$Q_e = \frac{Q_m b C_e}{1 + bC_e} \tag{6}$$

$$\frac{1}{Q_e} = \frac{1}{Q_m b C_e} + \frac{1}{Q_m} \tag{7}$$

In the formula, C_e (mg/L) represents the concentration at adsorption equilibrium. b represents the Langmuir adsorption equilibrium constant. Q_e (mg/g) is the adsorption capacity at adsorption equilibrium. Q_m denotes saturated adsorption (mg/g). Here, the values of b and Q_m are calculated according to the intercept and slope of the line drawn by C_e/Q_e on the graph of C_e.

In addition, the separation factor parameter R_L is commonly used to represent the basic features of Langmuir's equation, which is calculated by the following formula; see Equation (8).

$$R_L = \frac{1}{1 + bC_0} \tag{8}$$

where C_0 (mg/L) represents the initial concentration. The separation factor parameter R_L represents the type of isotherm.

Figure 6b shows the fitting curve of the Langmuir model of MPBNs. Table S1 lists the parameters of the Langmuir model. It can be seen from the figure that $1/Q_e$ and $1/C_e$ conformed to a linear relationship, with the linear fitting line of $1/Q_e = 0.10032/C_e + 0.05873$ and the determination coefficient $R^2 = 0.9750$. Moreover, the calculated values of Q_m and b were 17.0270 mg/g and 0.1003 L/g, respectively. The results indicated that the adsorption behavior of MPBNs for cesium ions comprised monolayer adsorption on the surface, and the medium on the surface of the MPBNs was uniformly distributed. In addition, R_L values were calculated according to Equation (8), and it can be seen in Table S2 that the R_L values of separation factor parameters ranged from 0.0168 to 0.4059, indicating that MPBNs displayed a favorable adsorption process for cesium ions.

The Freundlich model considers that the adsorption process belongs to multi-layer adsorption, and the adsorbent has different adsorption sites on the adsorbate, which belongs to the non-homogeneous adsorption process. Its calculation equation is as follows; see Equation (9). The linear expression of Freundlich's model is shown in Equation (10).

$$Q_e = KC_e^{1/n} \tag{9}$$

$$LnQ_e = LnK + (LnC_e)/n \tag{10}$$

In the formula, Q_e (mg/g) represents the adsorption capacity at adsorption equilibrium; C_e (mg/L) represents the concentration at adsorption equilibrium. K represents Freundlich's constant related to the adsorption capacity. n represents the constant of the surface interaction strength and adsorption tendency of adsorption molecules and adsorbents in Freundlich. The value of $1/n$ can be used to evaluate the adsorption performance.

When $0 < 1/n < 1$, the adsorption is favorable. When $1/n > 1$, the adsorption is unfavorable. Here, the values of K and n can be obtained by calculating the slope and intercept of the line obtained from the plot of LnC_e by LnQ_e.

Figure 6c exhibits the fitting curve of experimental data using the Freundlich model, showing the variation relationship between LnQ_e and LnC_e. Table S1 lists the parameters of Freundlich's model. Its linear fitting equation is $LnQ_e = 0.70854\ LnC_e + 1.65794$, $R^2 = 0.9791$. The calculated values of K and $1/n$ were 5.2785 mg/g and 0.7085, respectively. Among them, $1/n < 1$, so the MPBNs had a good affinity for cesium ions, which also indicates that MPBNs can easily adsorb cesium ions.

The Temkin model holds that the adsorbates interact with each other during the adsorption process, which indirectly affects the adsorption equilibrium to some extent. Because of this interaction, the molecular adsorption heat of each layer will decrease with the increase in coverage, which will lead to its linear relationship [35]. The Temkin model considers that the interaction between adsorbates causes the heat of adsorption between molecules to decrease continuously, and also considers that the surface of the adsorbent has homogeneous adsorption [36]. The calculation formula of the Temkin model is as follows; see Equation (11). Its linear expression is shown below in Equation (12).

$$Q_e = BLn\ (AC_e) \tag{11}$$

$$Q_e = BLnA + BLnC_e \tag{12}$$

In the formula, Q_e (mg/g) represents the adsorption capacity at adsorption equilibrium. C_e (mg/L) represents the concentration at adsorption equilibrium. B and A (L/mg) represent Temkin's constants. Here, the values of B and A can be obtained by calculating the slope and intercept of the line obtained from Q_e's plot of LnC_e. A is related to the heat of adsorption.

Figure 6d displays the Temkin model fitting curve of MPBNs for cesium ions, indicating the variation relationship between Q_e and LnC_e. Table S2 lists the parameters of the Temkin model. The linear fitting equation of the Temkin model was $Q_e = 8.42922LnC_e + 6.80233$, and the determination coefficient $R^2 = 0.9205$. The values of A and B were 2.2412 and 8.4292 (L/g), respectively.

The adsorption isotherms of MPBNs were fitted using the above three adsorption models and the determination coefficients (R^2) of the three adsorption models were compared. It was found that the determination coefficient R^2 of the Langmuir model and Freundlich model was greater than 0.95, which indicated that, within a certain concentration range, the adsorption isotherm of matrix-adsorbed metal ions can be fitted with two or more isotherm adsorption models. Moreover, the determination coefficient R^2 of the Freundlich adsorption model was the closest to 1, indicating that the adsorption of cesium ions by MPBNs was the most consistent with the Freundlich adsorption model. It was proven that the adsorption process of cesium ions by MPBNs belonged to multilayer adsorption and there were different adsorption sites, which indicated a heterogeneous adsorption process [37]. Moreover, the results indicated that MPBNs with nanostructures have a good affinity for cesium ions, and the adsorption process of cesium ions is favorable ($0 < 1/n = 0.7085 < 1$), being easier to carry out.

3.5. Adsorption Kinetics of MPBNs

In the adsorption process, the influence of the adsorption time on the adsorption capacity was as shown in Figure 7a. The results showed that the cesium ion adsorption was faster at the beginning of the 20 min period and reached equilibrium when the time increased to 60 min. In other words, as the time increased, the adsorption capacity did not change significantly. This not only indicated that the MPBNs had a strong adsorption capacity for cesium ions, but also that they can complete the adsorption process in a short time. Finally, 60 min was determined to be the equilibrium time of the adsorption reaction.

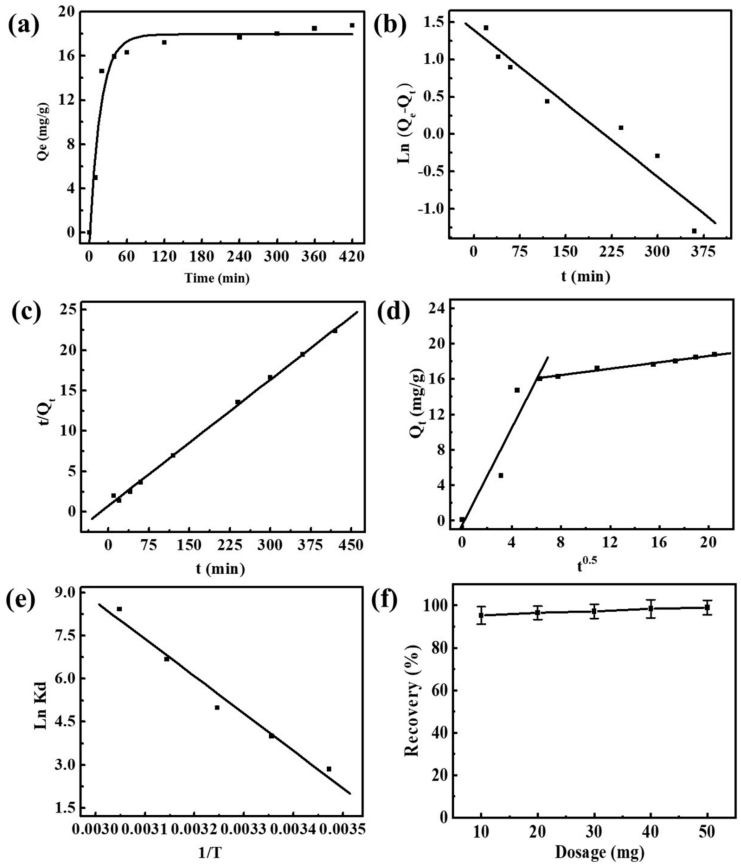

Figure 7. (**a**) Effect of time on adsorption amount of cesium ions (C_0 = 40 mg/L; pH = 5.5; m = 30 mg; V = 20 mL; T = 293 K); (**b**) pseudo-first-order reaction fit of cesium ion sorption kinetics by MPBNs; (**c**) pseudo-second-order reaction fit of cesium ion sorption kinetics by MPBNs; (**d**) the intraparticle diffusion reaction fit of cesium ion sorption kinetics by MPBNs; (**e**) Arrhenius plot for cesium ion adsorption by MPBNs; (**f**) effect of dosage for the recovery rate of MPBNs (C_0 = 40 mg/L; T = 293 K; pH = 5.5; V = 40 mL; t = 12 h).

To further discuss the speed control steps and kinetic laws in the adsorption process, this work used three kinetic equations—namely the quasi-first-order kinetic model, the quasi-second-order kinetic model, and the particle diffusion kinetic model—to fit the dynamics of MPBNs and study the relationship between the adsorption capacity of the adsorbent and the adsorption time in the adsorption process.

3.5.1. Dynamic Model

The quasi-first-order kinetic model assumes that the diffusion step controls the process of adsorption. During this process, the adsorption rate is proportional to the difference value between the respective adsorption amount at equilibrium and time t [38]. The quasi-first-order dynamic model equation is shown as follows; see Equation (13). When t = 0, Q_t = 0 and $t = t$, $Q_t = Q_t$ can be expressed as follows; see Equation (14).

$$\frac{dQ_t}{d_t} = K_1(Q_e - Q_t) \tag{13}$$

$$Ln\ (Q_e - Q_t\ ) = \ LnQ_e - K_1 t \tag{14}$$

where Q_e (mg/g) represents the adsorption capacity at adsorption equilibrium. Q_t (mg/g) represents the adsorption capacity at time t. K_1 represents the rate parameter of the quasi-first-order dynamic model. The values of Q_e and K_1 in the expression can be obtained by calculating the intercept and slope of the line plotted by t according to $Ln\ (Q_e - Q_t)$.

The quasi-first-order reaction kinetics equation was used to fit the experimental data of cesium removal by MPBNs at different times, and the linear equation was obtained, as shown in Figure 7b. The equation expression was $Ln\ (Q_e - Q_t) = 1.39387 - 0.00655t$, $R^2 = 0.9351$. The calculated values of K_1 and Q_e were 0.00655 min^{-1} and 4.0304 (mg/g), respectively. From the experimental results, it was found that the equilibrium adsorption amount was quite different from the actual adsorption amount, and the actual adsorption amount was relatively high. From the experimental results, it was found that the actual adsorption amount was approximately five times the equilibrium adsorption amount, and there was a large difference between them.

Next, the quasi-second-order kinetics model assumes that the chemisorption mechanism controls the adsorption rate in the adsorption process, and this chemisorption process involves electron sharing or electron transfer between adsorbents and adsorbates in the adsorption reaction [39]. The quasi-second-order dynamics model equation is shown as follows; see Equation (15). When $t = 0$, $Q_t = 0$ and $T = t$, $Q_t = Q_t$, the expression of the quasi-second-order dynamic model is derived as follows; see Equation (16).

$$\frac{dQ_t}{dt} = K_2(Q_e - Q_t)^2 \tag{15}$$

$$\frac{t}{Q_t} = 1/\left(Q_e^2 K_2\right) + t/Q_e \tag{16}$$

where Q_e (mg/g) represents the adsorption capacity at adsorption equilibrium. Q_t represents the adsorption capacity at time t (mg/g). K_2 represents the rate parameter (g/min·mg) of the quasi-second-order dynamics model. The values of Q_e and K_2 can be calculated from the intercept and slope of the line plotted by $Ln\ (Q_e - Q_t)$ against t. K_2 can reflect the rate of adsorption. If the adsorption process conforms to this kinetic model, a straight line can be obtained, and the whole adsorption process can be explained without knowing many parameters in advance.

The quasi-second-order fitting of the cesium adsorption kinetics is shown in Figure 7c. All the data in this figure were on a straight line, indicating that the experimental results conformed to the quasi-second-order kinetic equation. At this time, the linear expression of the equation was $t/Q_t = 0.76012 + 0.05211t$, $R^2 = 0.9979$. It was calculated that $K^2 = 0.003572$ g/mg·min^{-1}, $Q_e = 19.1902$ mg/g. Moreover, the determination coefficient R^2 of the quasi-second-order dynamics was the closest to 1, indicating that the adsorption of cesium ions by MPBNs was the most consistent with the quasi-second-order dynamics model. In other words, the theoretical value was consistent with the experimental data, which indicated that the adsorption process of cesium ions by MPBNs involved chemisorption, and the chemical strength was changed through ion exchange between MPBNs and cesium.

3.5.2. Diffusion Dynamics Model of Particles

Here, Q_t (mg/g) represents the adsorption capacity at time t. K_3 represents the diffusion kinetic rate constant of particles (g/g·$min^{1/2}$). C represents the constant of the particle's diffusion dynamics model. When Q_t is plotted against $t^{0.5}$, the slope and intercept of the line obtained are calculated. If there are multiple fitting lines in the drawing, it indicates that the adsorption process involves distributed adsorption [40].

The fitting results of the particle diffusion dynamics model are shown in Figure 7d, and the parameters of the model are shown in Table 1. It can be found from the figure that there are two particle diffusion curves of MPBNs adsorbing cesium ions, indicating that the adsorption process is distributed. The first step was the transport process of cesium ions outside the MPBNs, and the rate was affected by the solid–liquid diffusion velocity on the surfaces of the MPBNs. Moreover, the linear equation was $Q_t = 0.18028t^{0.5} + 15.00628$, and the determination coefficient $R^2 = 0.9753$. The second step was the mass transfer process of cesium ions in MPBNs, which was mainly affected by the diffusion rate in the nanospheres. In addition, the linear equation was $Q_t = 2.72081t^{0.5} + 0.61698$, and $R^2 = 0.8907$. Finally, there were two stages in the fitting curve. In the first stage, the line showed a good linear

relationship, and the fitting determination coefficient R^2 was close to 1. Furthermore, in the second stage, the diffusion rate constant K_{i2} was much smaller than in the first phase regarding the external diffusion rate constant K_{i1} (Table 1). It was shown that the diffusion rate of cesium ions into the nanospheres was significantly faster than that of the MPBNs during the adsorption process. Hence, the adsorption rate was affected by the inner and outer diffusion rates of MPBNs.

Table 1. Parameters reflecting the sorption kinetics, calculated using the kinetic models.

Adsorption Kinetic Model	Related Parameters	Linear Equations and Determination Coefficients
Quasi-first-order dynamics	K_1 (1/min) = 0.00655 Q_e (mg/g) = 4.0304	$Ln\ (Q_e - Q_t) = 1.39387 - 0.00655t$ $R^2 = 0.9251$
Quasi-second-order dynamics	K_2 (g/mg·min^{-1}) = 0.003572 Q_e (mg/g) = 19.1902	$t/Q_t = 0.76012 + 0.05211tR$ $^2 = 0.9979$
Particle diffusion (1)	K_{i1} (mg/g·min$^{0.5}$) = 0.18028 C = 15.00628	$Q_t = 0.18028t^{0.5} + 15.00628$ $R^2 = 0.9753$
Particle diffusion (2)	K_{i2} (mg/g·min$^{0.5}$) = 2.72081 C = 0.61698	$Q_t = 2.72081t^{0.5} + 0.61698$ $R^2 = 0.8907$

3.6. Adsorption Thermodynamics of MPBNs

Any adsorption process is associated with changes in system energy, so the thermodynamic parameters are the basic indicators of the spontaneity of the adsorption reaction process, including the Gibbs free energy (ΔG), enthalpy change (ΔH), and entropy change (ΔS). Meanwhile, the energy change in the adsorption process determines whether the adsorption process can be carried out spontaneously [41]. It is of great significance to further understand the role of the adsorbent by calculating various parameters of adsorption thermodynamics. This is because the solute is transferred from the solution to the solid–liquid contact interface by diffusion, which causes a change in the thermodynamic parameters (ΔG, ΔH and ΔS) in the process of adsorption. The adsorption thermodynamics calculation formula is as follows; see Equations (17)–(19).

$$K_d = Q_e/C_e \tag{17}$$

$$\Delta G = -RT\ LnK_d \tag{18}$$

$$LnK_d = \Delta S/R - \Delta H/RT \tag{19}$$

where Q_e (mg/g) represents the adsorption capacity at adsorption equilibrium. C_e (mg/L) represents the concentration at adsorption equilibrium. K_d represents the distribution coefficient in the adsorption process. R (8.314 J/mol/K) denotes the gas constant. T (K) represents the absolute temperature in the adsorption process. ΔH (kJ/mol) represents the amount of adsorption enthalpy. ΔS (J/mol/K) represents the Gibbs free energy. Through LnK_d, a straight line can be obtained with the $1/T$ slope ΔS and ΔH of numerical calculation.

To determine the adsorption thermodynamic parameters, the adsorption values at 288, 298, 308, 318, and 328 K were selected for calculation. Figure 7e shows the adsorption thermodynamic fitting curve of MPBNs adsorbing cesium ions, showing a good linear relationship. Moreover, the values of adsorption ΔG, ΔH, and ΔS of MPBNs are further listed in Table 2. The data showed that the ΔG of MPBNs was less than zero, which indicated that the adsorption behavior of cesium ions by the MPBNs was spontaneous and thermodynamic feasible [42]. Moreover, the absolute value of ΔG increased with the increase in temperature, which further proved that the increase in temperature was conducive to the adsorption of cesium ions by MPBNs. At the same time, ΔH was 108.15 kJ/mol, which was greater than zero, indicating that the adsorption involved the process of heat absorption. Moreover, ΔS had a value of 396.69 J/mol/K, and ΔS was greater than zero in the process of adsorption entropy increase. In the end, the adsorption was a process of entropy increase,

and the increase in entropy and enthalpy change were the driving forces in the adsorption process in the solid–liquid adsorption system.

Table 2. Adsorption thermodynamic data for the adsorption of cesium ions.

Temperature (K)	288	298	308	318	328
$-\Delta G$ (kJ/mol)	6.82	9.90	12.79	17.64	22.99
ΔH (kJ/mol)	108.15		ΔS (J/mol/K)	396.69	

3.7. Recovery Analysis of MPBNs

To further investigate the magnetic separation characteristics of MPBNs, the adsorbed cesium ions were recovered by magnetic separation, and we calculated the recovery rate [43]. The experimental results are shown in Figure 7f. Under the same conditions, the MPBNs after adsorption were recovered by magnetic separation. After calculation, when the initial dose of MPBNs was 10, 20, 30, 40, and 50 mg, the recovery rates were 95.27 ± 4.12%, 96.54 ± 3.15%, 97.19 ± 3.29%, 98.42 ± 4.31%, and 98.99 ± 3.45%, respectively. The experimental data showed that the recovery rates of all adsorbents were more than 95%, which proved that the MPBNs designed in this work had a good separation effect and recovery performance.

3.8. Comparison of Adsorption Capacity of MPBNs

The adsorption capacity of the MPBNs prepared in this work and other cesium ion adsorbents was compared, as shown in Table 3. Through comparison, it was found that the maximum adsorption capacity of MPBNs was greater than that of PB/A-SiO_2/PVDF and PB@Fe_3O_4 [7,44]. Although this cannot compare with the adsorption capacity of other adsorbents [45,46], it has the following advantages. On the one hand, compared with other magnetic materials [7,30,47], MPBNs have a strong magnetic force, short magnetic separation time and high recovery. Meanwhile, because Fe_3O_4 nanoparticles were embedded in the interior of PLA NPs, which can prevent the external environment from affecting its structure and play a protective role, the MPBN adsorbent can be applied at a wide range of pH values. On the other hand, GO and other MOF materials usually contain toxic metals [48], with complex preparation processes and poor economic benefits. On the contrary, MPBNs, in particular, use biodegradable PLA nanospheres.

Table 3. Comparison of sorption capacities of cesium ions on MPBNs and others.

Adsorbent	Maximum Adsorption Capacity (mg/g)	Reference
PB/A-SiO_2/PVDF	11.91	[44]
PB-MNC	45.87	[22]
PB/Fe_3O_4/GO	55.56	[30]
PB-coated ferriferous oxide	16.20	[49]
PB@Fe_3O_4	16.13	[7]
PVDF-PB-GO	20.07	[50]
GAC-COP-PB	1.091	[51]
PB-MCs	4.84	[18]
MPBNs	19.19	This work

4. Conclusions

In this work, oleic-acid-modified Fe_3O_4 NPs were prepared by the coprecipitation method, embedded in biodegradable PLA NPs, and PB NPs were fixed on their surfaces to obtain MPBN adsorbents. The results showed that the MPBNs were spherical, the average particle size was 268.2 ± 1.4 nm, the surface potential was −35.23 ± 1.59 mV, the saturation magnetization was 41.71 emu/g, and the iron content was 40.01%. When MPBNs were applied at 293 K, the maximum adsorption capacity of cesium was 19.12 mg/g, the suitable pH range was 5~9, and the reaction equilibrium time was 60 min. In addition,

the recovery rate of adsorbent was more than 95%. The adsorption isotherm was in line with the Freundlich isotherm model. The adsorption kinetics process conformed to the quasi-second-order fitting model. The adsorption process of MPBNs was jointly controlled by membrane diffusion and intraparticle diffusion. The thermodynamic study showed that the adsorption process was spontaneous and was an endothermic reaction. Increasing the temperature can improve the adsorption performance. According to the fitting results and experimental data, it was inferred that the reaction mechanism of cesium ion removal by MPBNs involved chemical adsorption, and the chemical strength was changed by ion exchange between MPBNs and cesium ions. MPBNs have good application prospects in the treatment of radioactive sewage by means of external magnetic field separation in water, providing technical support for the practical application of the Prussian blue adsorbent in cesium-containing wastewater.

Supplementary Materials: The following supporting information can be downloaded at: https://www.mdpi.com/article/10.3390/pr10122492/s1, Table S1: Parameters obtained from different isotherm models for MPBNs; Table S2: Parameters of the Cs^+ dimensionless separation factor (R_L) of the MPBNs.

Author Contributions: Conceptualization, S.F. (Shanshan Feng) and J.N.; funding acquisition, S.F. (Shanshan Feng), Y.Z. and F.M.; writing—original draft, J.N.; data curation, J.N. and J.G.; formal analysis, X.C. and F.M.; investigation, methodology, J.G.; resources, L.Y.; writing—review and editing, L.Y., X.C., W.J., F.C., S.F. (Sheng Feng) and Y.Z. All authors have read and agreed to the published version of the manuscript.

Funding: This research was funded by the Changzhou University Students' Extracurricular Innovation and Entrepreneurship Fund, the Natural Science Fund for Colleges and Universities in Jiangsu Province, the Science and Technology Project of Changzhou City, and the Natural Science Foundation of China and National Key Research and Development Program, grant numbers [ZMF21020079], [18KJB610001], [BK20180964], [CJ20210119], [2021D14013], [22075032], [2021YFC3001104], [2021YFC3001104], and [2021D14013], respectively.

Institutional Review Board Statement: Not applicable.

Informed Consent Statement: Not applicable.

Data Availability Statement: The experimental data involved in this work are listed in this paper, and the original data can be requested from the corresponding author.

Conflicts of Interest: The authors declare no conflict of interest.

References

1. Arai, H.; Fukushima, T.; Onda, Y. Radiocesium Accumulation in Lake Kasumigaura by Riverine Input and Migration Following the Fukushima Dai-Ichi Nuclear Power Plant Accident. *J. Environ. Manag.* **2022**, *320*, 115905. [CrossRef]
2. Liu, X.; Wang, J. Adsorptive Removal of Sr^{2+} and Cs^+ from Aqueous Solution by Capacitive Deionization. *Environ. Sci. Pollut. Res. Int.* **2021**, *28*, 3182–3195. [CrossRef] [PubMed]
3. Bondar, Y.; Olkhovyk, Y.; Kuzenko, S. Nanocomposite Adsorbent Based on Polyacrylonitrile Fibers for Rapid and Selective Removal of Cs Radionuclides. *J. Radioanal. Nucl. Chem.* **2021**, *330*, 1221–1231. [CrossRef]
4. Chenyang Yang, K.C. Rapid and Selective Removal of Cs^+ from Water by Layered Potassium Antimony Thiostannate. *J. Hazard. Mater.* **2021**, *403*, 124105. [CrossRef] [PubMed]
5. Kim, H.; Kim, M.; Kim, W.; Lee, W.; Kim, S. Photocatalytic Enhancement of Cesium Removal by Prussian Blue-Deposited TiO_2. *J. Hazard. Mater.* **2018**, *357*, 449–456. [CrossRef] [PubMed]
6. Ishizaki, M.; Akiba, S.; Ohtani, A.; Hoshi, Y.; Ono, K.; Matsuba, M.; Togashi, T.; Kananizuka, K.; Sakamoto, M.; Takahashi, A.; et al. Proton-Exchange Mechanism of Specific Cs+ Adsorption Via Lattice Defect Sites of Prussian Blue Filled with Coordination and Crystallization Water Molecules. *Dalton Trans.* **2013**, *42*, 16049–16055. [CrossRef] [PubMed]
7. Wang, P.; Zheng, J.; Ma, X.; Du, X.; Gao, F.; Hao, X.; Tang, B.; Abudula, A.; Guan, G. Electroactive Magnetic Microparticles for the Selective Elimination of Cesium Ions in the Wastewater. *Environ. Res.* **2020**, *185*, 109474. [CrossRef] [PubMed]
8. Lee, S.; Choi, M.; Moon, J.; Kim, S.; Lee, S.; Ryu, I.; Choi, J.; Kim, S. Electrosorption Removal of Cesium Ions with a Copper Hexacyanoferrate Electrode in a Capacitive Deionization (CDI) System. *Colloids Surf. A* **2022**, *647*, 129175. [CrossRef]
9. Torad, N.; Hu, M.; Imura, M.; Naito, M.; Yamauchi, Y. Large Cs Adsorption Capability of Nanostructured Prussian Blue Particles with High Accessible Surface Areas. *J. Mater. Chem.* **2012**, *22*, 18261–18267. [CrossRef]

10. Kim, H.; Kim, M.; Lee, W.; Kim, S. Rapid Removal of Radioactive Cesium by Polyacrylonitrile Nanofibers Containing Prussian Blue. *J. Hazard. Mater.* **2018**, *347*, 106–113. [CrossRef] [PubMed]
11. Thammawong, C.; Opaprakasit, P.; Tangboriboonrat, P.; Sreearunothai, P. Prussian Blue-Coated Magnetic Nanoparticles for Removal of Cesium from Contaminated Environment. *J. Nanopart. Res.* **2013**, *15*, 1689. [CrossRef]
12. Yang, H.; Li, H.; Zhai, J.; Sun, L.; Zhao, Y.; Yu, H. Magnetic Prussian Blue/Graphene Oxide Nanocomposites Caged in Calcium Alginate Microbeads for Elimination of Cesium Ions from Water and Soil. *Chem. Eng. J.* **2014**, *246*, 10–19. [CrossRef]
13. Feng, S.; Ma, F.; Liu, R.; Li, S.; Li, X.; Jin, Y.; Fu, G.; Yue, X. Highly Efficient Removal of Trace Level Dieldrin from Water Resources Utilizing a Cerasomal Strategy. *J. Mater. Chem. A* **2016**, *4*, 10263–10273. [CrossRef]
14. Li, S.; Ma, Y.; Yue, X.; Cao, Z.; Dai, Z. One-Pot Construction of Doxorubicin Conjugated Magnetic Silica Nanoparticles. *New, J. Chem.* **2009**, *33*, 2414–2418. [CrossRef]
15. Shokouhimehr, M.; Soehnlen, E.; Khitrin, A.; Basu, S.; Huang, S.D. Biocompatible Prussian Blue Nanoparticles: Preparation, Stability, Cytotoxicity, and Potential Use as an Mri Contrast Agent. *Inorg. Chem. Commun.* **2010**, *13*, 58–61. [CrossRef]
16. Shokouhimehr, M.; Soehnlen, E.; Hao, J.; Griswold, M.; Flask, C.; Fan, X.; Basilion, J.; Basu, S.; Huang, S. Dual Purpose Prussian Blue Nanoparticles for Cellular Imaging and Drug Delivery: A New Generation of T1-Weighted Mri Contrast and Small Molecule Delivery Agents. *J. Mater. Chem.* **2010**, *20*, 5251. [CrossRef]
17. Ke, H.; Wang, J.; Dai, Z.; Jin, Y.; Qu, E.; Xing, Z.; Guo, C.; Yue, X.; Liu, J. Gold-Nanoshelled Microcapsules: A Theranostic Agent for Ultrasound Contrast Imaging and Photothermal Therapy. *Angew. Chem. Int. Ed.* **2011**, *50*, 3017–3021. [CrossRef] [PubMed]
18. Feng, S.; Li, X.; Ma, F.; Liu, R.; Fu, G.; Xing, S.; Yue, X. Prussian Blue Functionalized Microcapsules for Effective Removal of Cesium in a Water Environment. *RSC Adv.* **2016**, *6*, 34399–34410. [CrossRef]
19. Jeon, C.; Cha, J.-H. Removal of Cesium Ions from Waste Solution Using Sericite Incorporated into Nickel Hexacyanoferrate. *Korean J. Chem. Eng.* **2015**, *32*, 2273–2279. [CrossRef]
20. Zarnegar, Z.; Safari, J. Modified Chemical Coprecipitation of Magnetic Magnetite Nanoparticles Using Linear–Dendritic Copolymers. *Green Chem. Lett. Rev.* **2017**, *10*, 235–240. [CrossRef]
21. Wu, Z.; Wang, M.; An, X.; Du, J.; Fan, H.; Lin, N.; Wang, Z.; Hao, X.; Guan, G. Intelligent Nanospheres with Potential-Triggered Undamaged Regeneration Ability and Superparamagnetism for Selective Separation of Cesium Ion. *Chem. Eng. J.* **2017**, *325*, 229–238. [CrossRef]
22. Yang, H.; Jang, S.; Hong, S.B.; Lee, K.; Roh, C.; Huh, Y.S.; Seo, B. Prussian Blue-Functionalized Magnetic Nanoclusters for the Removal of Radioactive Cesium from Water. *J. Alloys Compd.* **2016**, *657*, 387–393. [CrossRef]
23. Li, X.; Wu, X.; Chen, J.; Li, Y.; Yang, Y. Alginate-Enfolded Copper Hexacyanoferrate Graphene Oxide Granules for Adsorption of Low-Concentration Cesium Ions from Aquatic Environment. *J. Radioanal. Nucl. Chem.* **2019**, *320*, 655–663. [CrossRef]
24. Huang, G.; Chen, J.; Dou, P.; Yang, X.; Zhang, L. In Situ Electrosynthesis of Magnetic Prussian Blue/Ferrite Composites for Removal of Cesium in Aqueous Radioactive Waste. *J. Radioanal. Nucl. Chem.* **2020**, *323*, 557–565. [CrossRef]
25. Feng, S.; Cao, X.; Zheng, W.; Yue, X.; Li, X.; Li, S.; Wang, X.; Feng, S. In-Situ Formed Prussian Blue Nanoparticles Supported by Porous Biochar as Highly Efficient Removal of Cesium Ions. *J. Environ. Chem. Eng.* **2022**, *10*, 107972. [CrossRef]
26. Chieng, B.W.; Ibrahim, N.A.; Yunus, W.M.Z.W.; Hussein, M.Z. Poly(Lactic Acid)/Poly(Ethylene Glycol) Polymer Nanocomposites: Effects of Graphene Nanoplatelets. *Polymers* **2014**, *6*, 93–104. [CrossRef]
27. Xiong, L.; Huang, R.; Chai, H.; Yu, L.; Li, C. Facile Synthesis of Fe_3O_4@Tannic Acid@Au Nanocomposites as a Catalyst for 4-Nitrophenol and Methylene Blue Removal. *ACS Omega* **2020**, *33*, 20903–20911. [CrossRef]
28. Rauwel, P.; Rauwel, E. Towards the Extraction of Radioactive Cesium-137 from Water Via Graphene/Cnt and Nanostructured Prussian Blue Hybrid Nanocomposites: A Review. *Nanomater.* **2019**, *9*, 682. [CrossRef] [PubMed]
29. Miharaa, Y.; Sikder, M.T.; Yamagishi, H.; Sasaki, T.; Kurasaki, M.; Itoh, S.; Tanaka, S. Adsorption Kinetic Model of Alginate Gel Beads Synthesized Micro Particle-Prussian Blue to Remove Cesium Ions from Water. *J. Water Process Eng.* **2016**, *10*, 9–19. [CrossRef]
30. Yang, H.; Sun, L.; Zhai, J.; Li, H.; Zhao, Y.; Yu, H. In Situ Controllable Synthesis of Magnetic Prussian Blue/Graphene Oxide Nanocomposites for Removal of Radioactive Cesium in Water. *J. Mater. Chem. A* **2014**, *2*, 326–332. [CrossRef]
31. Lee, J.H.; Kwak, S. Mechanochemically Synthesized Prussian Blue for Efficient Removal of Cesium Ions from Aqueous Solutions. *ACS Omega* **2022**, *7*, 3222–3229. [CrossRef]
32. He, Y.; Yang, Y.; Huang, Z.-Y.; Wang, W.; Li, X.; Zhang, P.; Tan, Z.; Zhang, D. One-Pot Fabrication of Ferric Ferrocyanide Functionalized Graphene Hydrogel for Cesium Removal in Aqueous Solution. *RSC Adv.* **2017**, *7*, 45085–45092. [CrossRef]
33. Lai, Y.; Chang, Y.; Chen, M.; Lo, Y.; Lai, J.; Lee, D. Poly(Vinyl Alcohol) and Alginate Cross-Linked Matrix with Immobilized Prussian Blue and Ion Exchange Resin for Cesium Removal from Waters. *Bioresour. Technol.* **2016**, *214*, 192–198. [CrossRef] [PubMed]
34. Chen, G.; Chang, Y.; Liu, X.; Kawamoto, T.; Tanaka, H.; Kitajima, A.; Parajuli, D.; Takasaki, M.; Yoshino, K.; Chen, M.; et al. Prussian Blue (Pb) Granules for Cesium (Cs) Removal from Drinking Water. *Sep. Purif. Technol.* **2015**, *143*, 146–151. [CrossRef]
35. Nnadozie, E.; Ajibade, P. Data for Experimental and Calculated Values of the Adsorption of Pb(Ii) and Cr(Vi) on Aptes Functionalized Magnetite Biochar Using Langmuir, Freundlich and Temkin Equations. *Data Brief* **2020**, *32*, 106292. [CrossRef]
36. Lin, L.; Li, Y.; Wan, J.; Liu, C.; Wang, X.; Yin, Y. Efficient Trapping of Cesium Ions in Water by Titanate Nanosheets: Experimental and Theoretical Studies. *Water Pract. Technol.* **2021**, *16*, 1128–1140. [CrossRef]

37. Voronina, A.; Orlov, P.; Mashkovtsev, M.; Semenishchev, V. The Study of Mechanism of Cesium Sorption by Modified Aluminosilicates. *AIP Conf. Proc.* **2018**, *2015*, 020112.
38. Arun, T.; Joseyphus, R.J. Prussian Blue Modified Fe3o4 Nanoparticles for Cs Detoxification. *J. Mater. Sci.* **2014**, *49*, 7014–7022. [CrossRef]
39. Jang, S.; Haldorai, Y.; Lee, G.; Hwang, S.; Han, Y.; Roh, C.; Huh, Y.S. Porous Three-Dimensional Graphene Foam/Prussian Blue Composite for Efficient Removal of Radioactive Cs-137. *Sci. Rep.* **2015**, *5*, 1–10. [CrossRef]
40. Dwivedi, C.; Pathak, S.K.; Kumar, M.; Tripathi, S.C.; Bajaj, P.N. Preparation and Characterization of Potassium Nickel Hexacyanoferrate-Loaded Hydrogel Beads for the Removal of Cesium Ions. *Environ. Sci. Water Res. Technol.* **2015**, *1*, 153–160. [CrossRef]
41. Jung, Y.; Choi, U.S.; Ko, Y.G. Securely Anchored Prussian Blue Nanocrystals on the Surface of Porous Paam Sphere for High and Selective Cesium Removal. *J. Hazard. Mater.* **2021**, *420*, 126654. [CrossRef] [PubMed]
42. Bok-Badura, J.; Jakóbik-Kolon, A. Cesium Ion Sorption on Hybrid Pectin-Prussian Blue Beads: Batch and Column Studies to Remove Radioactive Cesium from Contaminated Wastewater. *Hydrometallurgy* **2022**, *213*, 105937. [CrossRef]
43. Yang, H.; Park, C.; Lee, K.; Lee, B.; Kim, I.; Yoon, I. Polyvinyl Alcohol-Borate Hydrogel Containing Prussian Blue for Surface Decontamination. *J. Radioanal. Nucl. Chem.* **2018**, *316*, 955–962. [CrossRef]
44. Liu, H.; Wang, H.; Yang, Y.; Ye, Z.; Kuroda, K.; Hou, L. In Situ Assembly of PB/SiO_2 Composite Pvdf Membrane for Selective Removal of Trace Radiocesium from Aqueous Environment. *Sep. Purif. Technol.* **2021**, *254*, 117557. [CrossRef]
45. Zhang, H.; Hodges, C.S.; Mishra, P.K.; Yoon, J.Y.; Hunter, T.N.; Lee, J.W.; Harbottle, D. Bio-Inspired Preparation of Clay–Hexacyanoferrate Composite Hydrogels as Super Adsorbents for Cs^+. *ACS Appl. Mater. Interfaces* **2020**, *12*, 33173–33185. [CrossRef]
46. El-Sherbeeny, A.; Ibrahim, S.; AlHammadi, A.; Soliman, A.; Shim, J.; Abukhadra, M. Effective Retention of Radioactive Cs^+ and Ba^{2+} Ions Using B-Cyclodextrin Functionalized Diatomite (B-Cd/D) as Environmental Adsorbent; Characterization, Application, and Safety. *Surf. Interfaces* **2021**, *26*, 101434. [CrossRef]
47. Jang, J.; Lee, D.S. Magnetic Prussian Blue Nanocomposites for Effective Cesium Removal from Aqueous Solution. *Ind. Eng. Chem. Res.* **2016**, *55*, 3852–3860. [CrossRef]
48. Jiang, Z.; Liu, G.; Ma, C.; Guo, Y.; Duo, J.; Li, M.; Deng, T. Cesium Removal from Wastewater: High-Efficient and Reusable Adsorbent $K_{1.93}Ti_{0.22}Sn_3S_{6.43}$. *Chemosphere* **2022**, *305*, 135406. [CrossRef] [PubMed]
49. Sasaki, T.; Tanaka, S. Magnetic Separation of Cesium Ion Using Prussian Blue Modified Magnetite. *Chem. Lett.* **2012**, *41*, 32–34. [CrossRef]
50. Zhang, Y.; Wang, H.; Gao, K.; Huang, D.; Hou, L.A.; Yang, Y. Efficient Removal of Cs(I) from Water Using a Novel Prussian Blue and Graphene Oxide Modified Pvdf Membrane: Preparation, Characterization, and Mechanism. *Sci. Total Environ.* **2022**, *838*, 156530. [CrossRef] [PubMed]
51. Seo, Y.; Hwang, Y. Prussian Blue Immobilized on Covalent Organic Polymer-Grafted Granular Activated Carbon for Cesium Adsorption from Water. *J. Environ. Chem. Eng.* **2021**, *9*, 105950. [CrossRef]